

35. Kegel, G., Reichwein, B., Wesse, S., Gaus, Peter-Katalinic, J. and Keller, R., *FEBS Lett.*, 1989, **255**, 10–14.  
 36. Webster, S. G., *Proc. R. Soc. London*, 1991, **B244**, 247–252.  
 37. Tensen, C. P., De Kleijn, D. P. V. and Van Herp, F., *Eur. J. Biochem.*, 1991, **200**, 103–106.  
 38. Keller, R., *Experientia*, 1992, **48**, 439–448.

<sup>^</sup>ACKNOWLEDGEMENTS: Unpublished observations reported in this paper are supported by DFG, Germany. T. Subramoniam is grateful to the Indian National Science Academy and DFG for the exchange of Scientist Visitorship to Bonn.

Received 18 November 1992; revised accepted 7 May 1993

## RESEARCH ARTICLE

# Petrology of tectonically segmented Central Indian Ridge

R. Mukhopadhyay and S. D. Iyer

National Institute of Oceanography, Dona Paula, Goa 403 004, India

**Distribution and mineralogy of various rock types along the 4200-km-long slow-spreading Central Indian Ridge, between Owen fracture zone in the north and Indian Ocean triple junction in the south, is studied in the light of ridge segmentation, and associated stress regime. To understand such phenomena along an extremely low magmatic budget spreading axis, rock samples from nine sites were examined. Rocks at these sites differ markedly in mineralogical composition and texture, but, surprisingly, not geochemically. Nature of segmentation of the ridge (length and offset) by transform faults appears to have influenced the variable extent of melting of the source rock and depth of magma generation below each ridge segment. We conclude that segmentation plays a significant role in facilitating polybaric fractional crystallization and the resultant mineralogical and textural variations in the erupted rocks.**

THE old understanding of magma chamber configuration being a 'relatively large, essentially molten, steady-state reservoir in which melt accumulates and undergoes magmatic differentiation prior to eruption or emplacement'<sup>1</sup> has undergone a distinct change to 'relatively small (<1 km thick, 1–3 km wide), tectonically bounded, lenticular magma chambers surrounded by semi-molten low-seismic-velocity zone (LVZ)<sup>2</sup>. Recent reports suggest that proximity to structural offsets such as transform faults could lead to a lower magmatic temperature<sup>3</sup>, a wide range of magma composition<sup>4</sup> and the resultant eruption of the enriched basalt<sup>5</sup>. Thus, it appears that transform fault separates coherent geochemical units reflecting differences in crystal fractionation and extents of melting. A concept

of 'spreading cell-deval' has been proposed to account for an observation<sup>5</sup> of such small magma chambers. (A small ridge portion bounded by two transform faults is known as a spreading cell, which also describes the boundary of smaller magma chambers<sup>2, 4, 5</sup>.)

In continuation to such understanding, we examine here the effects of small and large transform faults on the petrology of Mid-Ocean Ridge Basalts (MORB) and magmatic processes along the less explored, slow-accreting Central Indian Ridge (CIR). The geologic settings and petrology of rocks dredged from nine sites along the 4200-km-long ridge system [from the Owen fracture zone (OFZ) in the northwest to the south up to Indian Ocean triple junction (IOTJ)] are described. Bathymetric data from these sites (Figure 1), along a number of profiles across the ridge system, were collected by narrow-beam echo-sounder and Seabeam systems, onboard the research vessels, viz. *ORV Sagar Kanya* (India), *RV Sonne* (Germany) and *Academician Vernadskiy* (Russia). These sites correspond to three tectonic environments: zone I, sites located at or near large offset (> 55 km) of the ridge by transform faults (sites A, D, F and G); zone II, sites located at and around small offsets (10–55 km) of the ridge by transform faults (sites C, E and H); and zone III, midway along relatively undisturbed rift valley floor of individual tectonic segment (RVF, sites B and I). The average water depth of the sampled sites is 3225 m (range 4664 m at A to 1700 m at D; Table 1). A little more than 4500 kg of rocks were recovered from 33 dredge operations at the nine sites. For seven of these sites petrological examination was made, while for sites A and D the earlier description was followed<sup>6</sup>.

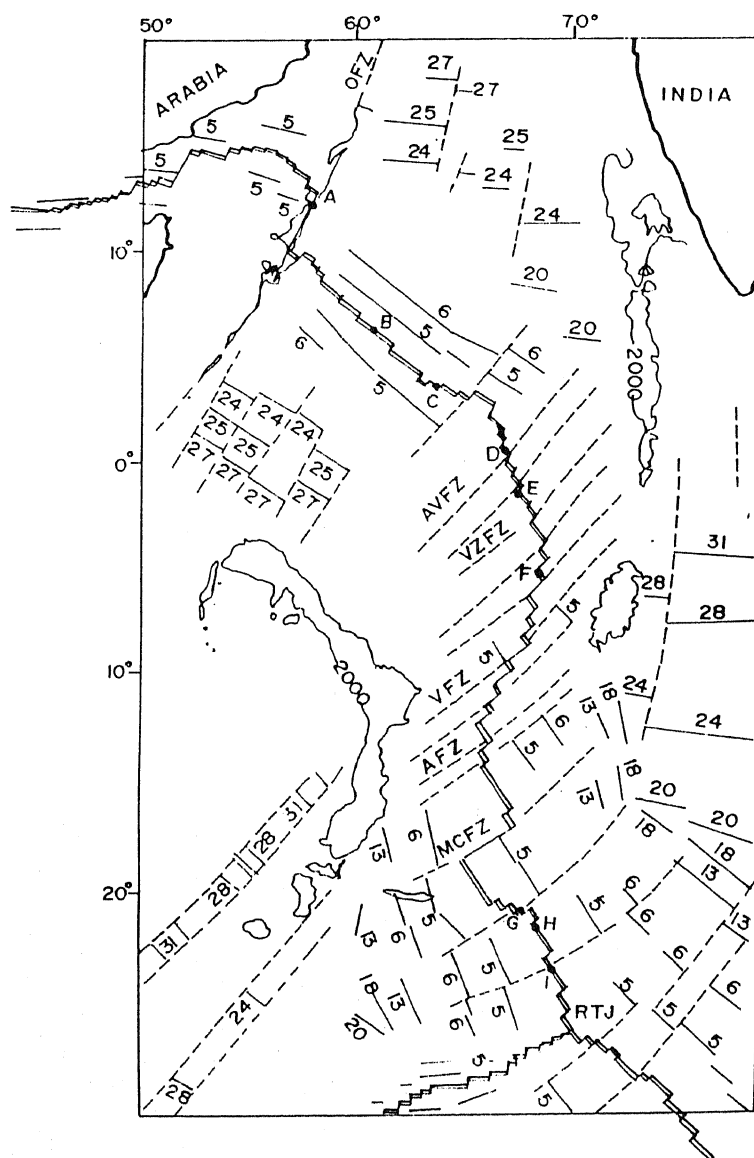


**Figure 1.** Bathymetric contour of 2000 m depth, and tectonic configuration of Central Indian Ridge. (.) represents nine sampling sites (A to I) from Owen fracture zone (OFZ) to Indian Ocean triple junction (IOTJ). Fracture zones, viz. AVFZ = Academician Vernadskiy, VZFZ = Vityaz, VFZ = Vema, AFZ = Argo, MCFZ = Marie Celeste, are shown. Solid lines with numbers indicate magnetic anomalies. (Base map after Royer *et al.*<sup>24</sup>.)

## Geologic settings

We consider the CIR as being made up geographically of two sections: the section between OFZ and the equator is termed as the Carlsberg ridge (CR), and the section between the equator and the IOTJ as the South Indian ridge (SIR). The IOTJ, where the African-Indian-Antarctica plates meet, is approximately situated at 25°S and 70°E, marking the southern tip of the CIR. We describe below the morphology of the CIR system under three different tectonic settings.

### Zone I (large offsets of the ridge, > 55 km)

The CIR system has undergone major horizontal and vertical displacements throughout its 4200 km length as

exemplified distinctly at sites A, D, F and G (Figure 1; Table 1). Site A, marking the northern end of the CIR system, occurs along OFZ at the intersection of Sheba ridge on the Arabian plate and CR. The OFZ, running NNE-SSW, displaces the CIR-Arabian ridge by ~ 340 km. The density of underlying rocks indicates a positive gravity anomaly, distorted locally by lower values<sup>6</sup>. Site D occurs on a 57-km-long segment close to the intersection of Academician Vernadskiy fracture zone (AVFZ) and the CR. Although AVFZ extends for a much longer length (~ 600 km), the displacement of the rift axis has remained low (~ 71 km). In addition to horizontal displacement, vertical emplacement occurs here with a 35-km-long ultramafic block uplifted to 1311 m on the rift axis from a surrounding valley floor depth of 4100 m. This is

Table 1. Structural and petrological characteristics of the nine studied sites

Site location Water depth	Geologic setting	Ridge offset (km)	Segment length (km)	Texture	Rock types and mineralogy	Source
A 12°10'N 4664 m	Uplifted LO	340	—	—	Serpentinized peridotite	Kalyayev <i>et al.</i> <sup>6</sup>
B 06°09'N 4034 m	RVF	NO	230	Subophitic, intersertal, intergranular	P(34), and-lab, twinned, fluid incl. O(18), subhedral; Px (3), Diop-Augt, V(2), M(43)	Pluger <sup>7</sup> Present study
C 03°35'N 3300–4100 m	SO	51	57	Glassy, porphyritic, spherulitic, variolitic	P (dominant, belt-buckle, sector zoned), O (medium- to fine-grained), Px (rare)	Banerjee and Iyer <sup>11,12</sup> Present study
D 01°37'N 1700–4100 m	Uplifted LO	71	57	—	Ultramafics, chrome spinels	Kalyayev <i>et al.</i> <sup>6</sup>
E 01°30'S 3457 m	SO	54	85	Quench, spherulitic, flow	P (21), Carlsbad twin, fractured, wavy extinction, O (9) anhedral, Px (tr), V(4) empty, irregular, M(66)	Pluger <sup>7</sup> , Present study
F 05°22'S 2084 m	LO	83	57	Intergranular	P (28), phenocryst, O (16), Px (2), M (64)	Pluger <sup>7</sup>
G 20°30'S 3776 m	LO	69	85	1) Porphyritic, quench 2) Variolitic	P (42), megacrysts, laths, bent O (18), deformed, replaced by Augt, Px (10), M&V (30), dark globules in vesicles P (27), quenched, O (9), euhedral, altered, Px (1), M (63).	Present study Present study
H 21°20'S 2499–3586 m	SO	50	170	Spherulitic, variolitic	P (20), alb-byt, phenocryst, fractured O (8), altered, fan-shaped, M&V (72).	Pluger <sup>7</sup> , Herzig and Plugger <sup>10</sup> , Present study
I 23°S 3354 m	RVF	NO	190	Flow, microporphyritic, variolitic	P (14), phenocryst, O (5), altered, V&M (81), Spinel, hematite	Pluger <sup>7</sup> , Herzig and Plugger <sup>10</sup> , Present study

RVF, rift valley floor; LO, large offset of ridge (> 55 km); SO, small offset (10–55 km); NO, no offset; P, plagioclase; O, olivine; Px, pyroxene; Diop, diopside; augt, augite; V, vesicles; M, matrix; and-lab, andesine-labradorite; alb-byt, albite-bytownite. Figures in parentheses indicate modal percentages in the rocks.

corroborated by a large negative gravity anomaly<sup>6</sup>. Site F is located at the tip of a locally displaced (offset 83 km) segment (length 57 km) of the SIR. The extension of the ridge system here is asymmetrical, with very steep eastern side and gentler western side<sup>7</sup>. Site G, with a well-developed, wide (40–50 km) median valley (length of segment 85 km) trending N30°W, shows high-amplitude central magnetic anomaly (350–400 nT). The median valley is offset (~69 km) by left-lateral strike slip movement along a newly identified transform fault<sup>8</sup>. North of the offset the median valley is 25 km wide and 2 km deep, while in the south it reduces to less than 1 km deep.

#### Zone II (small offset of the ridge, 10–55 km)

Three sites (C, E and H; Figure 1; Table 1) fall under this tectonic category. Site C occurs on a segment (length

57 km) characterized by offset (51 km) along a right lateral strike slip direction, a rare phenomenon on the CIR<sup>9</sup>. Bathymetric studies across the rift axis here indicate an asymmetrical widening of the ridge system. At site E, a number of transform faults of different lengths intersect the CIR at various angles, possibly causing in turn the change in orientations of the rift axis from NW–SE to N–S. The segment covering site E is 85 km long and is offset by 54 km by transform fault. At site H, the ridge flanks are 8–10 km wide, and rise to 2700 m (western flank) and 2400 m (eastern flank). The asymmetrical rift valley shallows from >3500 m in NW to ~3100 m in SW, with a central circular high occurring at 21°25'S and 68°46'E and a lateral offset of the ridge axis by about 4 km. Several volcanic cones more than 200 m high occur throughout the rift valley. Segment H extends for 170 km in length and is offset by ~50 km by fracture zones.

Zone III

Sites B and I (Figure 1; Table 1), apparently devoid of any ridge offsets, represent typical rift valleys. At site B, the CR widens asymmetrically, the southern part being gentler and more extended<sup>7</sup>. This site occurs on a long segment of 230 km. Site I is bordered by a transform fault in the north and the segment in which it occurs is ~ 190 km. A central longitudinal high of 300 m within the valley extends for about 15 km towards southeast. This high divides the median valley into a wide and deep (> 3800 m) western valley and a narrow and shallow eastern valley. The axial valley narrows from 12 km in the north to 8 km in the south. The ridge flanks are fissured and fractured, with openings from few cm to meter wide, and steep normal faults with displacement of few meters also occur<sup>10</sup>.

Petrology

The principal rocks found along the CIR system are basalts and ultramafics (Table 1). The more crystalline pillow fragments and talus form 90% of the collected rock samples while sheet flow basalts account for the rest. The size of the rocks recovered varies from 1 cm to ~ 20 cm. Some fragments show various hues on their fresh surfaces as a result of seawater-rock interactions<sup>11</sup>. The recovered samples in few cases show fresh glass up to 1 cm thick, have 1-3 mm deposit of ferromanganese oxides, and clay-like alteration products of a mixture of smectite and Ca-zeolite<sup>10</sup>.

Rocks dredged from zone I are ultramafics at sites A and D and pillow and sheet lava at site F. The ultramafics include serpentinized peridotites, talc-anthophyllite and lherzolites. These rocks show effects of vertical displacement and dynamic metamorphism as evident from slickensides, breccias and calcitic cements<sup>6</sup>. Rocks collected from zone II are composed mostly of pillow lavas which are striated and form protuberances. Rocks collected from zone II are generally fresh, glassy sheet flows and pillow lavas.

Results of the textural and mineralogical studies are given in Table 1. Mineralogically, the rocks are moderately phryic plagioclase basalts, with plagioclase as the dominant mineral, followed by olivine and pyroxene, and with varying proportion of groundmass materials (Figure 2). Anorthite content of plagioclase gradually increases in rocks of SIR. Zoned plagioclase is more common in basalts from the CR section (site C)<sup>12, 13</sup> than from the other sites. Olivine, with slightly higher percentage of abundance, shows a proportional relation to pyroxene (Figure 2) uptill 20°S, beyond which the abundance of plagioclase and olivine reduces while that of pyroxene and groundmass increases.

A decrease in olivine occurrence is seen in tectonically disturbed ridge areas (zones I and II). Olivine (Fo 84-88,

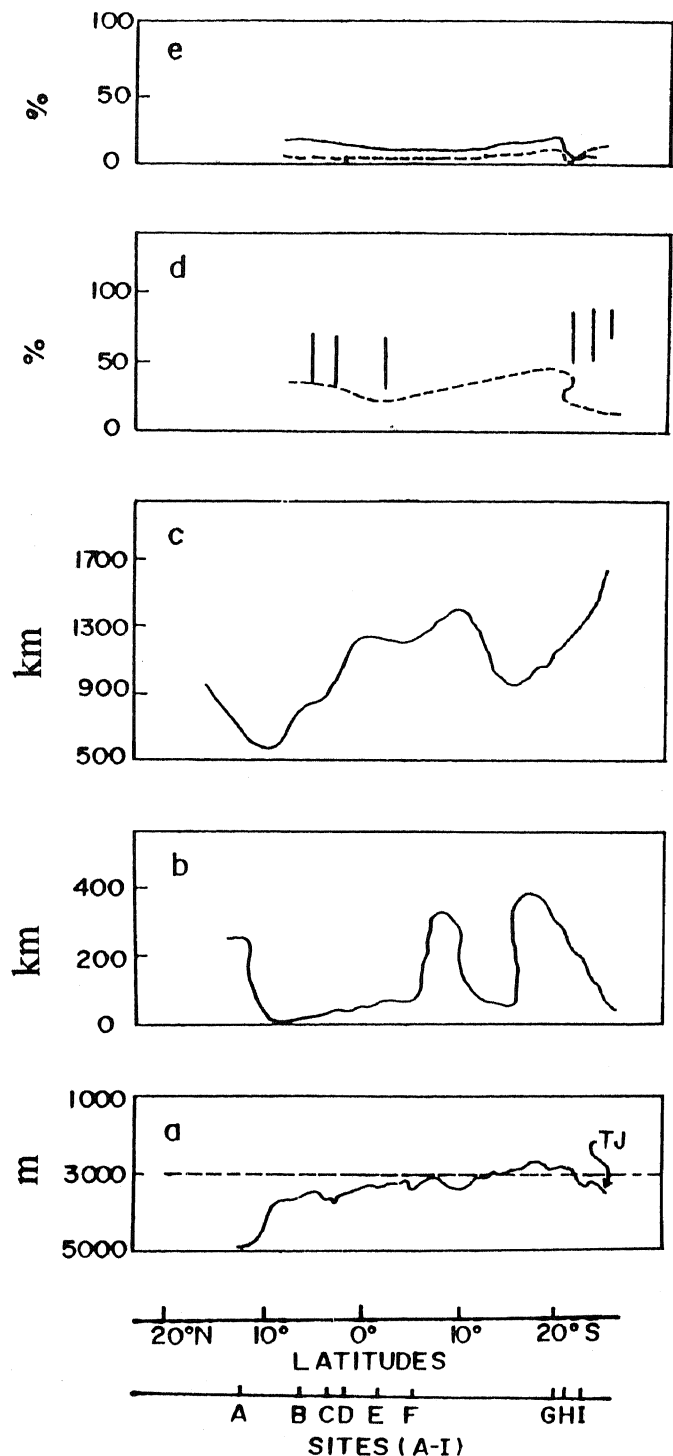


Figure 2. Tectonic characteristics of and mineral assemblage at sites A to I. a, Depth of rift valley (TJ = Triple junction); b, offsets (in km) of rift axis by fracture zones; c, length of the fracture zones; d, modal percentage of plagioclase phenocrysts (---) and range of anorthite content in plagioclase (vertical lines); e, modal percentage of phenocrysts of olivine (---) and pyroxene (—).

avg. Fo 86) occurs within the crystalline upper and lower parts of the sheet flows and in crystalline pillow margins<sup>10</sup>.

Microprobe analyses of plagioclase and olivine from site C basalts indicate the plagioclase phenocrysts and microphenocrysts to have An = 82–87 mol%, and the laths to have An = 67–79 mol%, while Fo content of olivine varies from 83 to 91 mol%, indicating low-pressure equilibrium crystallization<sup>13</sup>.

## Discussion

It is well known that seafloor spreading rate controls the gross morphology of rift axis and spreading centre. The CIR is a slow-spreading ridge (average rate < 5 cm/yr), and represents all the characteristics typical of slow-spreading ridges. The RVF is deep, wide, (2.8–4.5 km; Figures 1 and 2) rugged, faulted and shows a discontinuous axial neovolcanic zone (seen prominently at site I). A long period of quiescence in eruption consequent to the low rate of magma supply<sup>14</sup> between major eruptive cycles, which presumably occur after every 5000 to 10,000 years<sup>15</sup>, is responsible for such characteristics.

In the north the transform faults are more frequent but nonlinear compared to those in the south. These parameters seem to be influenced by the rate of spreading. In the north, the nonuniform rate of seafloor spreading even in close proximity (2.4–2.8 cm/yr between 8° and 4°N, ref. 16) indicates a zone of considerable tectonic stress. This nonuniformity in spreading rate is further manifested by the bending of the CIR system from NW–SE to N–S just north of the equator, and by a change in orientation of transform faults intersecting the CIR. The orientation of transform faults changes from N30E at 11°N to N60E at 20°S through N52E at 9°S, N57E at 13.5°S and N60E at 16°S (ref. 16). On the contrary, the rate of seafloor spreading (4.9–5.2 cm/yr from 20.3 to 24.3°S; ref. 16) and linearity of the rift valley increase towards south of the equator. Nonlinearity of the CIR is also suggested as being due to the differential rate of compensation of the oceanic crust at Java–Sumatra trench in the northeast and beneath the Eurasian plate in the north<sup>17</sup>. Furthermore, episodic volcanisms along the CIR could result in nonuniform stress and strain regimes, resulting in nonlinearity of the CR and the SIR systems<sup>9, 14</sup>. The faults (5–30 km in length along the strike) are formed by failure of crust during spreading under tension, rather than by cracking due to thermal contraction<sup>18</sup>.

We find some correlations between degree of offsets of the CIR by transform faults and petrology. At sites A and D, vertical displacements are as enormous as horizontal ones, bringing up the ultramafics onto the sea floor. Compressional and tensional stresses developed along the fracture zones, in response to change in the spreading direction, are a major cause for vertical tectonic activities<sup>6, 19</sup>. Besides these, movements on low-angle normal faults could also unroof deep structural levels locally along slow-spreading ridges<sup>20</sup>.

Mineralogically, rocks from sites F and G contain quite high abundance of phenocrysts of plagioclase and olivine (Figure 2). Pyroxene is also present in these rocks, which is mostly uncommon in rocks from other areas except at site B. High abundance of phenocrysts and the presence of plagioclase + olivine + pyroxene paragenesis indicates solidification from a moderately fractionated melt which has experienced a long cooling time. This situation was largely facilitated by transform faults with large offsets (sites F and G) and by being on the valley floor (site B).

Plagioclase enrichment in MORB can be related to rate of spreading and to depth of crystallization<sup>21</sup>. Accumulation of Ca-rich plagioclase (Table 1) in our study area can be accomplished in two ways: (i) by gravitational settling at the bottom of magma chambers and (ii) by floating due to increase in pressure on magma chambers. At slow-spreading ridges such as the CIR (< 5 cm/yr), accumulation of calcic plagioclase is probably a high-pressure effect of polybaric fractionation<sup>21</sup>. Polybaric fractionation at the CIR encompasses two stages occurring at 15–25 km and < 5 km depth below the seafloor<sup>22</sup>. Mixing of these high- and low-pressure magmas probably explains the mineral assemblages in the basalts studied.

Thus, the present suite of samples from the slow-spreading CIR bear signatures of polybaric crystallization, accumulation of calcic plagioclase phenocrysts, different depths of magma generation and rampant zoning in plagioclase phenocrysts. These signatures suggest their origin from small, buoyant magma chambers. Again, the variable presence of phenocrysts of olivine and plagioclase in the basalts at various sites indicates diversity in the composition of the parent liquid. Such diversity could come through variations in the depth of magma generation, extent of partial melting or degree of crystal separation, even if the original mantle material were similar<sup>21</sup>.

Geochemically, the basaltic rocks along the length of the CIR are not genetically dissimilar<sup>10, 13, 23</sup>. However, mineralogically and texturally these rocks do present dissimilar characteristics. The nature of transform faults and magnitude of ridge offsets appear to have created local favourable physicochemical environments for the development of such anomalies. The concept of spreading cell is revoked for explaining the differential extent of partial melting coupled with variable depth of magma generation beneath each ridge segment. Under these conditions, different degrees of cooling, fractionation and segregation of magmatic melts have caused variations in MORB mineralogy (abundance of plagioclase and olivine) and texture (phenocrystic, zoning and melt inclusions) along the length of the CIR.

1. Dungan, M. A. and Rhodes, J. M., *Contrib. Mineral. Petrol.*, 1978, **67**, 417–431.
2. Sinton, J. M. and Detrick, R. S., *J. Geophys. Res.*, 1992, **97**, 197–216.

3. Christie, D. M. and Sinton, J. M., *Earth Planet. Sci. Lett.*, 1981, **56**, 321–355.
4. Langmuir, C. and Bender, J. F., *Earth Planet. Sci. Lett.*, 1984, **69**, 107–127.
5. Langmuir, C., Bender, J. F. and Batiza, R., *Nature*, 1986, **322**, 422–429.
6. Kalyayev, G. I., Karabovich, S. V., Rusakov, O. M. and Startostenkov, V. I., *Geotectonics*, 1983, **17**, 32–42.
7. Pluger, W. L., *Fahrtbericht SO-28 und Wissenschaftlicher Bericht GEMINO-I: Geothermal Metallogenesis Indian Ocean*, 1988, p. 274.
8. Chaubey, A. K., Krishna, K. S., Subba Raju, L. V. and Rao, D. G., *Deep-Sea Res.*, 1990, **37**, 647–656.
9. Mitchell, N. C. J., *J. Geophys. Res.*, 1991, **96**, 8019–8043.
10. Herzig, P. M. and Pluger, W. L., *Can. Mineral.*, 1988, **26**, 721–736.
11. Banerjee, R. and Iyer, S. D., *Indian J. Mar. Sci.*, 1989, **18**, 124–127.
12. Banerjee, R. and Iyer, S. D., *J. Geol. Soc. India*, 1991, **38**, 369–386.
13. Iyer, S. D. and Banerjee, R., *Geo-Mar. Lett.*, 1993, **13**, 153–158.
14. Macdonald, K. C., Scheirer, D. S. and Carbotte, S. M., *Science*, 1991, **253**, 986–994.
15. Atwater, T. M., in *Deep Drilling Results in the Atlantic Ocean* (eds. Talwani, M., Harrison, C. G. and Hayes, D. E.), Am. Geophys. Union, 1979, pp. 233–242.
16. Minister, J. B. and Jordan, T. H., *J. Geophys. Res.*, 1978, **83**, 5331–5354.
17. Mukhopadhyay, R. and Khadge, N. H., *Proc. Indian Acad. Sci. (Earth Planet. Sci.)*, 1990, **99**, 357–365.
18. Macdonald, K. C., *Annu. Rev. Earth Planet. Sci.*, 1982, **10**, 155–190.
19. Bonatti, E. and Hamlyn, P. R., in *The Sea* (ed. Emiliani, C.) John Wiley and Sons, New York, 1981, vol. 7, pp. 241–283.
20. Mutter, J. C. and Karson, J. A., *Science*, 1992, **257**, 627–634.
21. Flower, M. F. J., *Nature*, 1980, **287**, 530–532.
22. Green, D. H. and Ringwood, A. E., *Contrib. Mineral. Petrol.*, 1967, **15**, 103–190.
23. Klein, E. M. and Langmuir, C. H., *J. Geophys. Res.*, 1987, **92**, 8089–8115.
24. Royer, J. Y., Sclater, J. G. and Sandwell, D. T., *Proc. Indian Acad. Sci. (Earth Planet. Sci.)*, 1989, **98**, 7–24.

ACKNOWLEDGEMENTS. We thank R. R. Nair for suggestions, other members of GIOTAS group Drs R. Banerjee, S. M. Karisiddaiah and A. V. Mudholkar for help in the initial stages of this work, and U. Javali for drafting the figures. R. M. thanks CSIR for deputing him to participate in the GEMINO cruises onboard *FS Sonne*. We thank the referee for a helpful review.

Received 20 March 1993; revised accepted 21 May 1993

## RESEARCH COMMUNICATIONS

### Resistivity studies of metal complexes of lignocaine hydrochloride

A. Indira, S. B. Bellad, A. M. Babu, M. A. Sridhar and J. Shashidhara Prasad

Department of Studies in Physics, University of Mysore, Manasagangothri, Mysore 570 006, India

The temperature dependence of resistivities of the complexes lignocainehydrochloride–chromium (CRL), monochlorotrinitro copper(II) lignocaine (CUNL) and lignocainehydrochloride–manganese (MNL) has been studied. All the compounds exhibit semiconducting behaviour which can be accounted for by the stacking of the donor and acceptor molecules in the crystal structure. The degree of fall of resistivity of the compounds decreases in the order MNL, CRL, CUNL. The complex CUNL shows appreciable conductivity in the temperature range 234–279 K, as well as in the range 388–468 K. This behaviour might be attributed to the phase transition (if it exists) of the complex at a lower temperature.

LIGNOCAINE hydrochloride (LH), an important acetamide derivative, is commercially known by different names, viz. Xylocaine, Lidocaine and Gescicaine. Its chemical name is 2-(diethylamine)-*N*-(2,6-dimethylphenyl)acetamide hydrochloride. It is the most common and important local anaesthetic and anti-arrhythmic drug. In order to obtain a deeper insight into the function, activity and properties of

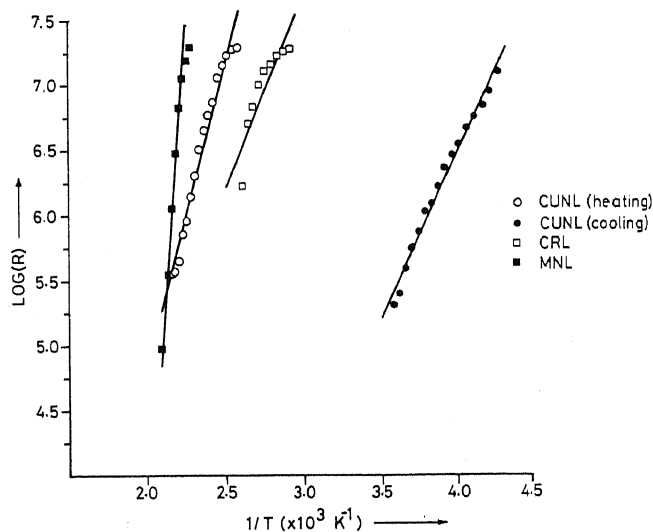


Figure 1.  $\log(R)$  vs  $1/T$  plot.

LH, we have taken up X-ray crystallographic studies of a number of charge transfer complexes of LH with various metals like Pt, Co, Cu, Fe, in the form of platinum chloride<sup>1</sup>, cobalt chloride<sup>2</sup>, copper chloride<sup>3</sup> and ferric chloride<sup>4</sup>. As a continuation of this, we have undertaken a study of the variation of resistivity as a function of temperature for lignocainehydrochloride–chromium complex (CRL), monochlorotrinitro copper(II) lignocaine complex (CUNL) and lignocainehydrochloride–manganese complex (MNL).